Numerical Simulation of Frequency-difference EIT using Multi-shell Concentric Spherical Head Model

Sujin Ahn[1], Sung Chan Jun[1] and Eung Je Woo[2]
[1]School of Information & Communications, Gwangju Institute of Science and Technology, Gwangju, KOREA
[2]Department of Biomedical Engineering, Kyung Hee University, Gyeonggi-do, KOREA
Email : scjun@gist.ac.kr

***Abstract*—We present numerical simulations of frequency-difference electrical impedance tomography (EIT) for imaging haemorrhagic stroke inside the head adopting a multi-shell concentric spherical head model. We performed a validation study of a weighted frequency-difference method through three-dimensional numerical simulations. Adopting the multi-shell model with a frequency-dependent admittivity distribution, we investigated the performance of the method to detect a blood anomaly. We found that the simple frequency-difference method fails to detect the anomaly whereas reconstructed images using the weighted frequency-difference method clearly visualize the anomaly. We found that the weighted frequency-difference method is robust against modeling errors since it is capable of detecting an anomaly surrounded by shell-shaped obstacles simulating the internal structures of the head. We propose the weighted frequency-difference method for future studies of animal and human experiments.**

Keywords : EIT, Electrical Impedance Tomography, Weighted frequency-difference EIT

I. Introduction

In electrical impedance tomography (EIT), we try to produce cross-sectional images of conductivity and permittivity distributions inside the human body. Injecting weak electric current into the body, an EIT system measures induced boundary voltages affected by the electrical properties of biological tissues. Applying an image reconstruction algorithm to the acquired voltage data, it displays images of the conductivity and/or permittivity distribution. Since conductivity values of biological tissues change with their physiological and pathological conditions, EIT is finding clinical applications in imaging pulmonary ventilation, haemorrhagic stroke, abdominal bleeding, breast tumor and others [5].

Reconstructed EIT images have a relatively low spatial resolution and may contain numerous artifacts. One of the most successful methods to reduce the artifacts is the difference imaging approach. In a time-difference EIT imaging method, voltage data sets measured at two different times are utilized to produce time-difference images. This kind of difference imaging method is advantageous since a data substraction process can cancel out unavoidable modeling errors and measurement artifacts common to both data sets.

Though the time-difference approach has been successfully applied to lung imaging, for example, it is not feasible for imaging tumor or bleeding since a time-referenced voltage data acquired in the absence of an anomaly is not available. Noting that different admittivity values of biological tissues change with frequency [1], [2], we may adopt a frequency-difference approach depending upon intended applications [3], [4], [8], [9], [11].

Lately, Seo etal (2008) proposed a weighted frequency-difference (WFD) algorithm instead of a simple frequency-difference (FD) method. The WFD method uses a weighted difference of two voltage data sets simultaneously acquired at two different frequencies whereas the FD method uses a simple voltage difference. They showed theoretically and numerically that a weighted voltage difference is required for an imaging object where its conductivity and/or permittivity distributions surrounding an anomaly change with frequency. Jun etal (2009) tested the WFD method in two-dimensional numerical simulations and phantom experiments and validated that the WFD method is superior to the FD method.

Since the EIT image reconstruction problem is inherently three-dimensional, the proposed WFD method must be validated in a three-dimensional setting. In this paper, we performed a numerical simulation study of detecting a hemorrhagic stroke in a three-dimensional human head model. We considered a blood anomaly located in a four-shell concentric spherical head model representing the scalp, skull, cerebrospinal fluid (CSF) and brain. We will show how this multi-shell model with different tissue conductivity values influences the performance of the frequency-difference EIT method.

II. Methods

A. Settings for Numerical Simulations

We considered the following four-shell spherical model in cm unit:

- Layer 1 $= \{(x,y,z)|\ 9.2^2 < x^2+y^2+z^2 \leq 10^2\}$
- Layer 2 $= \{(x,y,z)|\ 8.7^2 < x^2+y^2+z^2 \leq 9.2^2\}$
- Layer 3 $= \{(x,y,z)|\ 8.3^2 < x^2+y^2+z^2 \leq 8.7^2\}$
- Layer 4 $= \{(x,y,z)|\ x^2+y^2+z^2 \leq 8.3^2\}$

The layers 1 to 4 correspond to the scalp, skull, cerebrospinal fluid (CSF) and brain, respectively (Fig. 1(a)). We attached twenty seven electrodes on the outmost surface of the

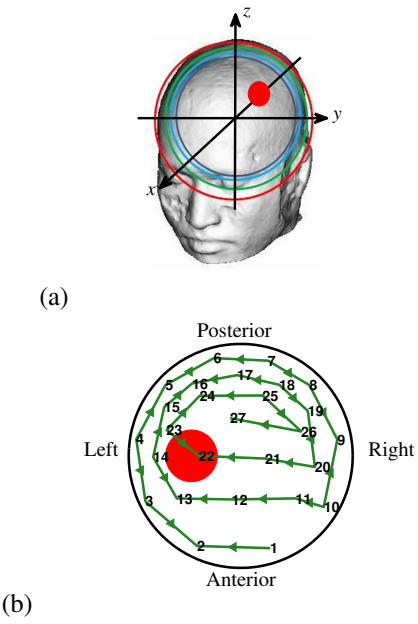

Fig. 1: (a) Sphere model with four layers. The blood anomaly was located on the left of the head. (b) The pattern of current injections and voltage measurements in the view from the bottom. The red area represents the blood anomaly.

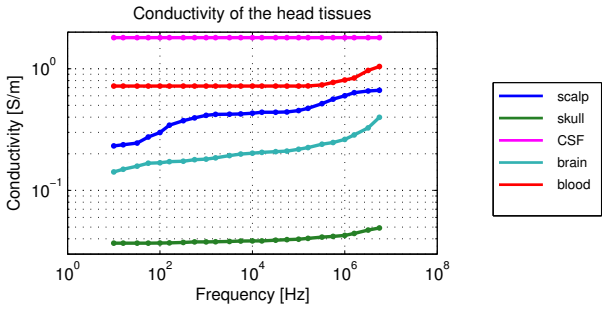

Fig. 2: Conductivity spectra of head tissues [6].

layer 1 according to the international 10-20 system (Fig. 1(b)). We considered the following two cases:

• Case 1 : we set the conductivity of the layer 2 as that of the skull and other layers have the conductivity of the brain.

• Case 2 : for all four layers, we set their conductivities as those of the scalp, skull, CSF and brain, respectively.

We used conductivity values of the head tissues as shown Fig. 2. We located a spherical blood anomaly at (0, 4.0, 4.5) in the left part of the head (Fig. 1(a)). The volume of the blood anomaly was 0.8% of the total volume of the sphere. We used a spiral data collection protocol with adjacent current injections and adjacent voltage measurements as illustrated in Fig. 1(b). In all simulations, we used five frequencies of 1, 5.6, 10, 56 and 100 kHz and added Gaussian noise of 20 dB signal-to-noise ratio (SNR) in voltage data. We produced frequency-difference images using the FD and WFD methods between two consecutive frequencies.

B. Image Reconstructions

We assume a three-dimensional imaging object denoted as Ω with its boundary $\partial\Omega$. Attaching electrodes E_j for $j = 1, \cdots, L$ on $\partial\Omega$, we inject a sinusoidal current $I\sin(\omega t)$ between a neighboring pair of electrodes E_j and E_{j-1}. This induces a complex harmonic voltage u_ω^j satisfying Eq. (1) where $\mathbf{r}$ is the position vector, z_k the contact impedance of the electrode E_k, $\mathbf{n}$ the outward unit normal vector on $\partial\Omega$, $V_\omega^{j,k}$ is the complex voltage on the surface of the electrode E_k and γ_ω the admittivity at frequency ω. We denote a data vector of measured boundary voltages as a column vector $\mathbf{f}_{t,\omega} = [f_{t,w}^{j,k}]$ where $f_{t,w}^{j,k} = V_{t,\omega}^{j,k} - V_{t,\omega}^{j,k-1}$ at time t and angular frequency ω where j and k are indices of the current-injection electrode pair and the voltage-measuring electrode pair, respectively. In this paper, all indices follow modulo operations, for example, $L+1 \to 1$.

$$\begin{cases} \nabla\cdot(\gamma_\omega(\mathbf{r})\nabla u_\omega^j(\mathbf{r})) = 0 \text{ in } \Omega \\ \left(u_\omega^j(\mathbf{r}) + z_k\gamma_\omega\frac{\partial u_\omega^j(\mathbf{r})}{\partial \mathbf{n}}\right) = V_\omega^{j,k} \quad \text{on } E_k,\ k = 1,\ldots,L \\ \gamma_\omega\frac{\partial u_\omega^j(\mathbf{r})}{\partial \mathbf{n}} = 0 \quad \text{on } \partial\Omega\backslash\cup_{k=1}^L E_k \\ \int_{E_k}\gamma_\omega\frac{\partial u_\omega^j(\mathbf{r})}{\partial \mathbf{n}}ds = 0 \quad \text{if } k \in \{1,\ldots,L\}\backslash\{j-1,j\} \\ \int_{E_j}\gamma_\omega\frac{\partial u_\omega^j(\mathbf{r})}{\partial \mathbf{n}}ds = I = -\int_{E_{j-1}}\gamma_\omega\frac{\partial u_\omega^j(\mathbf{r})}{\partial \mathbf{n}}ds \end{cases} \tag{1}$$

In the FD approach, we may first consider using a simple voltage difference $\mathbf{f}_{t,\omega_2} - \mathbf{f}_{t,\omega_1}$ at time t. We tentatively assume that the object is homogeneous, that is, $\gamma_{\omega_1}(\mathbf{r}) = \gamma_{\omega_1}$ and $\gamma_{\omega_2}(\mathbf{r}) = \gamma_{\omega_2}$. Since we assume in this paper that the admittivity changes with frequency, we should note that $\gamma_{\omega_1} \neq \gamma_{\omega_2}$. With $\bar{u}_{\omega_1}$ and $\bar{u}_{\omega_2}$, we denote the complex voltages satisfying Eq. (1) with γ_{ω_1} and γ_{ω_2} replacing $\gamma_\omega(\mathbf{r})$, respectively. We let $\bar{\mathbf{f}}_{t,\omega_1}$ and $\bar{\mathbf{f}}_{t,\omega_2}$ be the corresponding complex voltage data vectors at ω_1 and ω_2, respectively. Since Eq. (1) becomes the Laplace equation with the same boundary data for the homogeneous cases, $\gamma_{\omega_2}\bar{\mathbf{f}}_{t,\omega_2}$ is parallel to $\gamma_{\omega_1}\bar{\mathbf{f}}_{t,\omega_1}$ and we may express $\bar{\mathbf{f}}_{t,\omega_2} = (\frac{\gamma_{\omega_2}}{\gamma_{\omega_1}})\bar{\mathbf{f}}_{t,\omega_1}$. Even for the homogeneous case without any anomaly, $\bar{\mathbf{f}}_{t,\omega_2} - \bar{\mathbf{f}}_{t,\omega_1} \neq 0$ if $\gamma_\omega(\mathbf{r})$ changes with ω. Therefore, nonzero values of $\mathbf{f}_{t,\omega_2} - \mathbf{f}_{t,\omega_1}$ should be attributed to a global frequency-dependent admittivity change as well as a local change of an anomaly. Preferably, the frequency-dependent local change should be different from the frequency-dependent global change.

Let's assume that there exists a small anomaly inside a homogeneous imaging object. The admittivity of the anomaly differs from those of the background region at one or both of ω_1 and ω_2. From the smallness of the anomaly, we may approximate a nonzero voltage difference $\mathbf{f}_{t,\omega_2} - \mathbf{f}_{t,\omega_1} \approx \bar{\mathbf{f}}_{t,\omega_2} - \bar{\mathbf{f}}_{t,\omega_1} = \left(\frac{\gamma_{\omega_2}}{\gamma_{\omega_1}} - 1\right)\bar{\mathbf{f}}_{t,\omega_1}$. Effects of the local anomaly in the nonzero voltage difference $\mathbf{f}_{t,\omega_2} - \mathbf{f}_{t,\omega_1}$ will be easily overwhelmed by the global change term $\left(\frac{\gamma_{\omega_2}}{\gamma_{\omega_1}} - 1\right)\bar{\mathbf{f}}_{t,\omega_1}$. We should note that the global change term is proportional to the voltage data itself $\mathbf{f}_{t,\omega_1}$. This may result in increased image artifacts since the data subtraction process to cancel

out common errors does not operate.

The WFD method tries to annihilate the global change term to enhance the local contrast of the anomaly. We decompose $\mathbf{f}_{t,\omega_2} = \alpha\mathbf{f}_{t,\omega_1} + (\mathbf{f}_{t,\omega_2} - \alpha\mathbf{f}_{t,\omega_1})$ where α is a complex number. We may assume that $\alpha\mathbf{f}_{t,\omega_1}$ is a component of $\mathbf{f}_{t,\omega_2}$ which was mostly affected by the global admittivity change [7],[10]. To remove the global change term as much as possible, Seo et al. (2008) suggested to determine α which minimizes $\|\mathbf{f}_{t,\omega_2} - \alpha\mathbf{f}_{t,\omega_1}\|$. Since this is equivalent that $\mathbf{f}_{t,\omega_1}$ and $\mathbf{f}_{t,\omega_2} - \alpha\mathbf{f}_{t,\omega_1}$ are orthogonal to each other, the optimal value α^* is

$$\alpha^* = \frac{< \mathbf{f}_{t,\omega_2}, \mathbf{f}_{t,\omega_1} >}{< \mathbf{f}_{t,\omega_1}, \mathbf{f}_{t,\omega_1} >}$$

where $< \cdot, \cdot >$ is the inner product. In the WFD method, we use the weighted difference $\mathbf{f}_{t,\omega_2} - \alpha^*\mathbf{f}_{t,\omega_1}$ to produce a frequency-difference EIT image.

The sensitivity matrix was produced by the homogeneous sphere supposed to $\gamma(\mathbf{r}) = 1$ for all cases. So modeling errors caused by disagreement between a homogeneous sphere and a spherical model with 4 layered concentric shells were included in the computation of sensitivity matrix. We used the same sensitivity matrix for all cases. We used the singular value decomposition (SVD) of the matrix as $\mathbf{J} = \mathbf{U}\mathbf{\Sigma}\mathbf{V}^*$ where $\mathbf{U}$ and $\mathbf{V}$ are orthogonal matrices, * the Hermitian of a matrix and $\mathbf{\Sigma}$ a diagonal matrix of singular values. We produced a reconstructed image $\mathbf{g}_\lambda$ by the Tikhonov solution of

$$\mathbf{g}_\lambda = \mathbf{V}\mathbf{\Sigma}_\lambda^{-1}\mathbf{U}^*\Delta\mathbf{f}$$

where $\mathbf{\Sigma}_\lambda^{-1}$ is a diagonal matrix. The ith diagonal element of $\mathbf{\Sigma}_\lambda^{-1}$ is $\frac{s_i}{s_i^2+\lambda^2}$ for a positive constant λ and the ith diagonal element s_i of $\mathbf{\Sigma}$. The voltage difference $\Delta\mathbf{f}$ is one of $\mathbf{f}_{t,\omega} - \mathbf{f}_{0,\omega}$, $\mathbf{f}_{t,\omega_2} - \mathbf{f}_{t,\omega_1}$ and $\mathbf{f}_{t,\omega_2} - \alpha^*\mathbf{f}_{t,\omega_1}$. The regularization parameter λ satisfies $\mathbf{g}_\lambda = \arg\min_{\mathbf{g}} \|\mathbf{J}\mathbf{g} - \Delta\mathbf{f}\|^2 + \lambda^2\|\mathbf{g}\|^2$. We used Matlab (The Mathworks Inc., USA) for all computations and image generations. In each reconstructed image, we identified the anomaly as the biggest blob over the half-maximum conductivity change.

III. Results

We plot a reconstructed conductivity image in the view shown in Fig. 1(b). All images are shown in the axial plane passing through the center of the reconstructed anomaly. We considered the biggest blob over the half-maximum value as a reconstructed anomaly.

A. Images of Case 1

In the FD method, the global conductivity change around the skull layer strongly appeared all over the reconstructed images. The WFD method detected the blood anomaly on the left side with a small amount of artifacts. We can see that the modeling errors caused by ignoring the existence of the layer 2 shifted the reconstructed anomaly toward the left side and overestimated the size (Fig. 3).

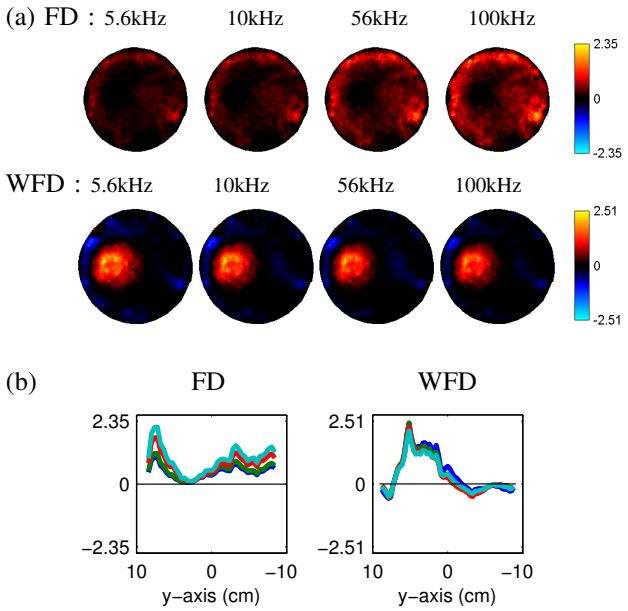

Fig. 3: (a) Axial images using the FD and WFD methods for Case 1. (b) Profiles passing through the center of the reconstructed anomaly. For each frequency-difference image, we used a reference frequency as the one just below the marked frequency.

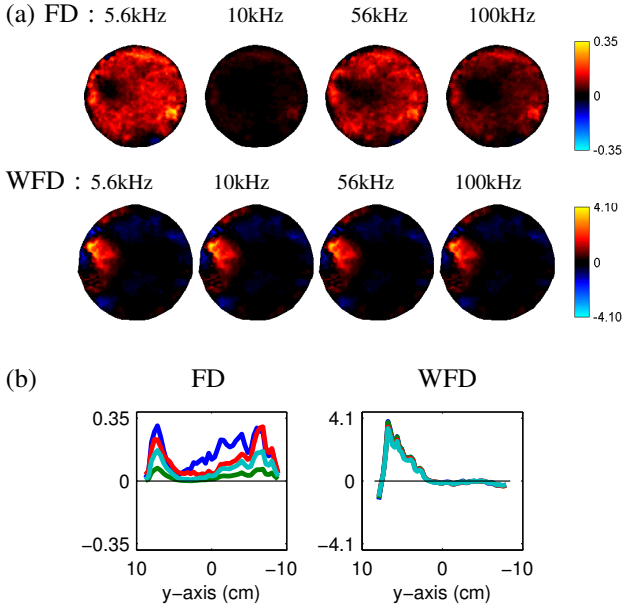

Fig. 4: (a) Axial images using the FD and WFD methods for Case 2. (b) Profiles passing through the center of the reconstructed anomaly. For each frequency-difference image, we used a reference frequency as the one just below the marked frequency.

B. Images of Case 2

Using the WFD method, we could successfully visualize the blood anomaly on the left side. However, we can observe more artifacts near the boundary and the anomaly position is shifted a little toward the posterior part. The FD method failed to detect the blood anomaly since the global conductivity change between two chosen frequencies dominated (Fig. 4).

IV. Discussion and Conclusion

We compared the FD and WFD methods in terms of their performance to detect a blood anomaly located in a four-shell concentric spherical head model. In frequency-difference imaging of stroke in the head, we must consider the inhomogeneous frequency-dependent conductivity distribution in the head. We found that the WFD method is always superior to the FD method when the background conductivity changes with frequency. From reconstructed FD images, we found that the artifacts due to the global change in the background conductivity with respect to frequency are more severe than those related with modeling errors we tested in this paper. The shell-shaped layer of a lower conductivity value tend to attenuate current densities inside the shell. We speculate that this caused the overestimation of the diameter of the reconstructed anomaly in WFD images in Fig. 3. We may attribute noticeable artifacts in images shown in Fig. 4 to the CSF conductivity which is almost ten times higher than those of the brain and other two layers (layer 2 and 3).

Since we produced the sensitivity matrix from a spherical model with a homogeneous conductivity distribution, our results must include modeling errors. The WFD method could handle such modeling errors and successfully detect the blood anomaly. In our future study, we plan to investigate a realistic head-shaped model followed by animal and human imaging experiments of the WFD method.

Acknowledgments

This work was supported by the NRF grant (2009-0071225) and the BioImaging research center at GIST. E J Woo was supported by the NRF grant (20100018275).

References

[1] S. Gabriel, R. W. Lau and C. Gabriel, "The dielectric properties of biological tissues: II. measurements in the frequency range 10 Hz to 20 GHz", *Phys. Med. Biol.* **41**, pp.2251-2269, 1996.

[2] L. A. Geddes and L. E. Baker, "The Specific Resistance of Biological Material - A Compendium of Data for Biomedical Engineer and Bphysiologist", *Med. & biol. Engng.* **5**, pp.271-293, 1967.

[3] H. Griffiths and A. Ahmed, "A dual-frequency applied potential tomography technique: computer simulations", *Clin. Phys. Physiol. Meas.* **8**, pp.103-107, 1987.

[4] H. Griffiths and Z. Zhang, "A dual-frequency electrical impedance tomography system", *Phys. Med. Biol.* **34**, pp.1465-1476, 1989.

[5] D. Holder (ed.) Electrical Impedance Tomography: Methods, History and Applications (Bristol, UK: IOP Publishing), 2005

[6] L. Horesh, "Some Novel Approaches in Modelling and Image reconstruction for Multi-Frequency Electrical Impedance Tomography of the Human Brain", Ph.D Thesis, UCL, 2006.

[7] S. C. Jun, J. Kuen, J. Lee, E. J. Woo, D. Holder and J. K. Seo, "Frequency-difference EIT (fdEIT) using weighted difference and equivalent homogeneous admittivity: validation by simulation and tank experiment", *Physiol. Meas.* **30**, pp.1087-1099, 2009.

[8] A. McEwan, A. Romsauerova, R. Yerworth R, L. Horesh, R. Bayford and D. Holder, "Design and calibration of a compact multi-frequency EIT system for acute stroke imaging", *Physiol. Meas.* **27**, S199-210, 2006.

[9] A. Romsauerova, A. McEwan, L. Horesh, R. Yerworth, R. H. Bayford and D. S. Holder, "Multi-frequency electrical impedance tomography (EIT) of the adult human head: initial findings in brain tumours, arteriovenous malformations and chronic stroke, development of an analysis method and calibration", *Physiol. Meas.* **27**, S147-161, 2006.

[10] J. K. Seo, J. Lee, S. W. Kim, H. Zribi and E. J. Woo, "Frequency-difference electrical impedance tomography (fdEIT): algorithm development and feasibility study", *Physiol. Meas.* **29**, pp.929-944, 2008.

[11] R. J. Yerworth, R. H. Bayford, B. Brown, P. Milnes, M. Conway and D. S. Holder, "Electrical impedance tomography spectroscopy (EITS) for human head imaging", *Physiol. Meas.* **24**, pp.477-489, 2003.